RSC Advances

PAPER

View Article Online
View Journal | View Issue

Cite this: *RSC Adv.*, 2024, **14**, 24534

Efficient phosphate removal utilizing N, Zn-doped carbon dots as an innovative nanoadsorbent†

Mina Alikhani,[a] Ehsan Khoshkalam, *[b] Jalal Sadeghi,[b] Laura Bulgariu[c] and Hossein Eshghi [d]

The primary goal of this study is to examine PO_4^{3-} adsorption from aqueous solutions using zinc-doped carbon dots (Zn-N-CDs) as a new adsorbent and cost-effective technique. Zn-N-CDs were produced through a hydrothermal process and subsequently identified using various techniques. The effect of reaction time, temperature, pH, ionic strength, adsorbent dosage, initial PO_4^{3-} concentration, and anion competition (NO_3^-, Cl^-, HCO_3^-, and SO_4^{2-}) on PO_4^{3-} adsorption using Zn-N-CDs were investigated. The characterization results depicted that Zn-N-CDs have a spherical structure without obvious aggregation and revealed the amorphous nature of carbon dots with many pores. Zn-N-CDs had a high affinity for adsorbing PO_4^{3-}, reaching equilibrium within 5 minutes. While PO_4^{3-} adsorption reduced with an increase in temperature, it increased with pH and ionic strength. The optimal conditions for PO_4^{3-} adsorption were determined to be pH 8, 100 mM KCl as an ionic strength, and 5 g L^{-1} of Zn-N-CDs. The presence of SO_4^{2-} and HCO_3^- as competing anions slightly decreased PO_4^{3-} adsorption. Thermodynamic studies revealed that PO_4^{3-} adsorption onto Zn-N-CDs was endothermic, spontaneous, and disordered, as evidenced by $\Delta G° < 0$, $\Delta H° > 0$, and $\Delta S° > 0$. The experimental data fit well with a pseudo-second-order kinetic model ($R^2 = 0.999$) and the Freundlich isotherm model ($R^2 = 0.9754$), signifying that PO_4^{3-} adsorption onto Zn-N-CDs occurs through multi-layer and chemi-sorption mechanisms. Overall, Zn-N-CDs indicated a great capability to adsorb high concentrations of PO_4^{3-} across a wide range of pH values, indicating their potential for environmental remediation.

Received 30th March 2024
Accepted 22nd July 2024

DOI: 10.1039/d4ra02428a

rsc.li/rsc-advances

1. Introduction

Agricultural practices, mining activities, and the utilization of synthetic detergents *etc.* are important sources of the pollutant PO_4^{3-} in the environment.[1,2] Environmental PO_4^{3-} abundance can be detrimental to humans, leading to kidney damage and osteoporosis.[2] Increasing PO_4^{3-} concentration in surface water promotes the growth of phosphate-dependent species such as algae and duckweed.[3] These organisms consume a lot of oxygen and keep sunlight out of the water. This makes the water inhospitable for other species. This phenomenon is often referred to as eutrophication.[2,3] Such conditions result in the demise of aquatic life, the production of odors, and the proliferation of harmful organisms.[3] Total PO_4^{3-} can range from 8.5 mg L^{-1} in landfill leachate to 740 mg L^{-1} in fresh urine, according to data found in the literature.[1,2] In addition, the recommended levels of total PO_4^{3-} in streams that reach lakes and flowing bodies of water are 0.05 and 0.1 mg L^{-1}, respectively.[1–3] Recovering PO_4^{3-} from aqueous environments could reduce these issues.

Over the last few decades, various techniques, including biological, chemical, and physical treatment processes have been utilized to remove PO_4^{3-}. However, these methods have become expensive and ineffective due to the production of sludge, the introduction of chemical reagents to the environment, and the generation of secondary harmful materials during the treatment process.[4] The biological technique, for instance, takes a long time and results in biological sludge. Additionally, some decontamination techniques, including chemical reduction, may produce hazardous byproducts.[5] To address these issues, scientists have turned their attention to adsorption treatment for water and wastewater purification. Adsorption techniques have proven to be highly efficient, sensitive, and selective in removing various organic and inorganic pollutants from water and wastewater.[1,2,4] Different types of adsorbents, including industrial and agricultural wastes,[6] polymeric exchangers,[7] EL-MNP@Zeolite,[8] La-CTS-ATP,[9]

[a]*Department of Chemistry, Payame Noor University, Tehran, Iran*

[b]*Department of Soil Science, Faculty of Agriculture, Ferdowsi University of Mashhad (FUM), Mashhad, Iran. E-mail: e.khoshkalam@alumni.um.ac.ir; Fax: +985138807147; Tel: +989104050217*

[c]*Department of Environmental Engineering and Management, Cristofor Simionescu Faculty of Chemical Engineering and Environmental Protection, Gheorghe Asachi Technical University of Iasi, 700050 Iasi, Romania*

[d]*Department of Chemistry, Faculty of Science, Ferdowsi University of Mashhad (FUM), Mashhad, Iran*

† Electronic supplementary information (ESI) available. See DOI: https://doi.org/10.1039/d4ra02428a

hydrotalcite,[10] and LDH[11] have been used for PO_4^{3-} removal. However, the high cost of producing and consuming these compounds, the multiple steps involved in the synthesis process, introducing harmful chemicals to the environment and the low efficiency in PO_4^{3-} adsorption are the disadvantages of such adsorbents.[12,13] Therefore, in order to be applicable at full scale, it is desirable to have environmentally friendly adsorbents.

The use of nanotechnology with the ability to produce nanoparticles with superior properties has been considered in surface absorption studies.[14,15] Among different nanoparticles, carbon based materials, including carbon dots (CDs) and graphene, have emerged as alternatives to conventional adsorbent materials. Carbon dots have been receiving increased interest due to their distinct optical properties, low toxicity, simple synthesis, extremely small size, high biocompatibility, and cost-effective precursors.[13,16,17] Owing to their distinctive physicochemical characteristics and the presence of numerous hydrophilic functional groups, CDs provide a multitude of surface adsorption sites to remove pollutants from the environment.[18,19]

Carbon dots have been utilized in numerous studies for the removal of heavy metals.[20–22] The capability of carbon dots to adsorb heavy metals primarily depends on their chemical properties, particular surface area, pore volumes, and the existence of functional groups.[22] Researchers have argued that the adsorption process of metal ions can occur due to physisorption, electrostatic attraction and chemical sorption.[13] Among these reactions, electrostatic attraction is considered pivotal in the adsorption mechanism between carbon dot-based adsorbents and metal ions, primarily due to the abundance of oxygen-containing groups with negative charges on the surface of these materials.[13] However, carbon dots have not been used as an adsorbent for removing PO_4^{3-}, and the reaction mechanism of these compounds with PO_4^{3-} ions remains unknown.

On the other hand, some research has reported that the combination of metal ions with carbon-based materials and LDH can generate additional surface functional groups and increase the efficiency of PO_4^{3-} adsorption.[1,10,11] For instance, Nakarmi *et al.*[1] by synthesized a zinc oxide-biochar nanocomposite, which removed 265.5 mg g^{-1} of PO_4^{3-} from water solutions. In another research, doping $Mn^{2+}/Zn^{2+}/Fe^{3+}$ oxy(-hydroxide) onto LDH, drastically increased the PO_4^{3-} adsorption, resulting in the adsorption of 82.3 mg g^{-1} of PO_4^{3-}. Furthermore, Koilraj and Kannan[10] argued that the presence of zinc ions in the ZnAl hydrotalcite could enhance PO_4^{3-} adsorption during chemi-sorption mechanisms.

Furthermore, the recent study showed that modifying carbon dots with zinc ions can alter their physical and chemical properties.[23] Based on our findings, so far no studies have been conducted regarding the adsorption of PO_4^{3-} by these types of nanoparticles. Therefore, to provide a precise answer to the question of whether the modification of carbon dots with zinc ions has the ability to retain PO_4^{3-} or not, this study aimed to prepare zinc-doped carbon dots (Zn-N-CDs), as a novel adsorbent for PO_4^{3-} adsorption from water solutions. The main objectives of this research were: (1) synthesizing and characterization of Zn-N-CDs, (2) evaluating PO_4^{3-} adsorption using Zn-N-CDs at different pH, electrolyte concentrations, and temperatures to determine the optimum dosage of the adsorbent, (3) investigating the kinetics, isotherms and thermodynamics studies of PO_4^{3-} adsorption, and (4) understanding the main mechanisms of PO_4^{3-} adsorption using Zn-N-CDs.

2. Materials and methods

2.1 Materials

$ZnCl_2$ (99%), citric acid ($C_6H_8O_7$, 99%), urea (CH_4N_2O, 99%), KCl (99.5%), NaOH (98%), K_2SO_4 (99%), KH_2PO_4 (99.5%), $KHCO_3$ (99.5%), and KNO_3 (99.5%) were all purchased from Merck, Germany, and are all of analytical grade. Also, double-distilled water was used to create each solution.

2.2 Preparation of Zn-N-CDs

The water-soluble Zn-N-CDs were synthesized using the previously described approach.[23,24] Briefly, 0.19 g (1 mmol) of citric acid and 0.12 g (2 mmol) of urea were dissolved in 15 mL of deionized water. Subsequently, the mixture was stirred at room temperature for 15 minutes. Then, the solution was added to a 5 mL aqueous solution of $ZnCl_2$ (1 mmol, 0.14 g) and stirred for 30 min. The aqueous solution was then placed in a Teflon autoclave, sealed, and heated for 12 h at 200 °C. The autoclave was then cooled to room temperature. The solution was centrifuged at 12 000 rpm for 20 min to remove excess reactants. To separate the black, insoluble particles, the resulting brown solution was filtered through a 0.45 μm filter membrane. The solution was then freeze-dried to obtain a dark brown Zn-N-CDs powder. The schematic of Zn-N-CDs synthesis is shown in Fig. S1.†

2.3 Characterization of Zn-N-CDs

The infrared spectra of KBr pellets were recorded using a PerkinElmer FT-IR spectrophotometer in the 400–4000 cm^{-1} region at standard ambient temperature. A field emission scanning electron microscope (FESEM, TESCAN MIRA3), was utilized to examine the surface structure and perform electron dispersive X-ray (EDS) analysis on the Zn-N-CDs. The UV-vis spectrophotometer Shimadzu UV-2550 was utilized for the analysis. Dynamic light scattering (DLS) and zeta potential (Malvern Zetasizer Nano ZS-90) was used to measure the particle size and surface charge of the Zn-N-CDs. The Zn-N-CDs structure was studied using a Zeiss transmission electron microscope (TEM). Measurements of fluorescence (FL) were taken using an F-7000 Hitachi spectrophotometer. The surface area and pore size characteristics of the Zn-N-CDs were determined using a Brunauer–Emmett–Teller (BET) analysis. The measurements were conducted using an ASAP 2020 apparatus (Micromeritics Instrument Corporation, USA), which is an Accelerated Surface Area and Porosity (ASAP) system.

2.4 Batch adsorption experiments

2.4.1 Determining optimal conditions. KH_2PO_4 was used to prepare PO_4^{3-} stock solution (1000 mg L^{-1}) and then diluted to the desired concentrations for further experiments. In these

experiments, optimal conditions of PO_4^{3-} adsorption using Zn-N-CDs were evaluated. Therefore, the effect of contact time (0–120 min), initial pH (2–12), ionic strength (1–100 mM KCl), Zn-N-CDs concentration (1–7 g L^{-1}), and initial PO_4^{3-} concentration (50–500 mg L^{-1}) were done, respectively. All solutions, with 10 mL final volume, were prepared in 25 mL glass bottles. For acquiring equilibrium time, the experiment (IS = 10 mM KCl, $[PO_4^{3-}] = 500$ mg L^{-1}, [Zn-N-CDs] = 3 g L^{-1}, without adjusting pH, 21 °C) was investigated at desired contact time. For evaluating the effect of temperature on phosphate adsorption, this experiment, with same condition as above, was performed at 35 °C and 45 °C, respectively.

In continue, the experiment was done in different pHs (2–12). The pH of solutions was adjusted using HCl/NaOH 0.1 M. Then, the optimum pH was used for further batch experiments. For investigating the effect of ionic strength, the adsorption PO_4^{3-} was tested at different KCl salt concentrations. The best ionic strength was then selected for determining of adsorbent dosage for PO_4^{3-} removal. Additionally, the effect of different background solutions, including KCl, NaCl, and $CaCl_2$, on PO_4^{3-} adsorption was evaluated. Finally, the effect of initial PO_4^{3-} concentration (50–500 mg L^{-1}) was evaluated under all optimal conditions. After sorption, all samples were centrifuged (10 000 rpm, 5 min) and the equilibrium PO_4^{3-} concentration was measured (using UV-spectrophotometer at a wavelength of 880 nm) at their supernatant.[5] The majority of the trials were done in triplicate. eqn (1) and (2) were used to achieve PO_4^{3-} adsorption in percent (R%) and q_t (mg g^{-1}), respectively.[5,10]

$$R(\%) = \frac{C_0 - C_t}{C_0} \times 100 \quad (1)$$

$$q_t = \frac{(C_0 - C_t)V}{W} \quad (2)$$

where V (L) is the volume of the solution and W (g) is the mass of the Zn-N-CDs utilized, C_0 (mg L^{-1}) and C_t (mg L^{-1}) are the residual concentrations of PO_4^{3-} at 0 and t (min) of reaction time, respectively.

2.4.2 Effect of competing anions on PO_4^{3-} adsorption. For this experiment, equal concentrations of anions ($[PO_4^{3-}]$, $[NO_3^-]$,$[Cl^-]$, $[HCO_3^-]$, and $[SO_4^{2-}] = 5.2$ mmol L^{-1}) were added to glass bottle containing 100 mM KCl and 5 g L^{-1} Zn-N-CDs (final volume = 10 mL). The glass bottles were centrifuged after being shaken for 5 minutes at 250 rpm. By using UV-spectrophotometer, the residual concentration of PO_4^{3-}, NO_3^-, and SO_4^{2-} was measured. The titrimetric method was used to determine the residual concentration of Cl^- and HCO_3^{5-}.

2.4.3 Kinetic, thermodynamic, and isotherm models. Three distinct kinetic models were used to establish the reaction control step, including the pseudo-first-order (eqn (3)), pseudo-second-order (eqn (4)), and intra-particle diffusion (eqn (5)) models.[5,11] Pseudo-first-order and pseudo-second-order models are frequently used to gather data on the equilibrium adsorption capacity of adsorbents, and the adsorption capacity is calculated using the model with the greatest correlation coefficient. The intraparticle diffusion model also establishes the rate-limiting property of intraparticle diffusion.[5,11]

$$\log(q_e - q_t) = \log q_e - \log\left(\frac{k_1 t}{2.303}\right) \quad (3)$$

$$\frac{t}{q_t} = \frac{1}{k_2 q_e^2} + \frac{t}{q_e} \quad (4)$$

$$q_t = k_p t^{1/2} + C \quad (5)$$

In these equations, the terms q_t, q_e, k_1, k_2, k_p, C, and t stand for the amounts of ions adsorbed at time t (mg g^{-1}), equilibrium time (mg g^{-1}), pseudo-first-order rate constant (min^{-1}), pseudo-second-order rate constant (mg min^{-1}), intra-particle diffusion rate constant (mg g^{-1} min^{-1}), intercept, and time (min), respectively.

In order to determining accurately adsorption capacity of Zn-N-CDs for PO_4^{3-} removal, adsorption data was fitted to the Freundlich (eqn (6)), Langmuir (eqn (7)), and Temkin (eqn (8)) isotherm models.[1]

$$\log(q_e) = \log(K_F) + \frac{1}{n}\log(C_e) \quad (6)$$

$$C_e/q_e = C_e/b + 1/K_L b \quad (7)$$

$$q_e = \frac{RT}{b_T}\ln K_T + \frac{RT}{b_T}\ln C_e \quad (8)$$

The equilibrium adsorption capacity and concentration of PO_4^{3-} at equilibrium are denoted by q_e (mg g^{-1}) and C_e (mg L^{-1}), respectively. The experimental constants K_F and $1/n$ are used in the Freundlich equation. The terms b (mg g^{-1}) and K_L in the Langmuir equation refer to the highest potential for adsorption and the constant of binding energy, respectively. b_T, K_T are the Temkin isotherm constants. R is the gas constant (J mol^{-1} K^{-1}) and T is the temperature (K). RT/B_T is the heat of adsorption (J mol^{-1}).

The adsorption process of PO_4^{3-} on the Zn-N-CDs was evaluated by calculating thermodynamics parameters including $\Delta G°$ (Gibbs free energy, kJ mol^{-1}), $\Delta H°$ (enthalpy change, kJ mol^{-1}), and $\Delta S°$ (entropy change, J mol^{-1} K^{-1}). These parameters were calculated as follow (eqn (9) and (10)).[11]

$$\Delta G° = -RT\ln K_d = -RT\ln\left(\frac{q_e}{C_e}\right) \quad (9)$$

$$\ln(K_d) = -\Delta H°/RT + \Delta S°/R \quad (10)$$

where q_e, C_e, R, T, and K_d are the amount of PO_4^{3-} adsorbed per unit of mass of the Zn-N-CDs (mg g^{-1}), concentration of PO_4^{3-} per unit volume of solution (mg L^{-1}), gas constant, temperature in Kelvin, and the distribution coefficient, respectively.

3. Results and discussion

3.1 Characterization

3.1.1 FT-IR spectroscopy. The FT-IR spectra were used to identify the functional groups on the Zn-N-CDs surface as well as the bond type (Fig. 1a). The FT-IR spectrum of Zn-N-CDs

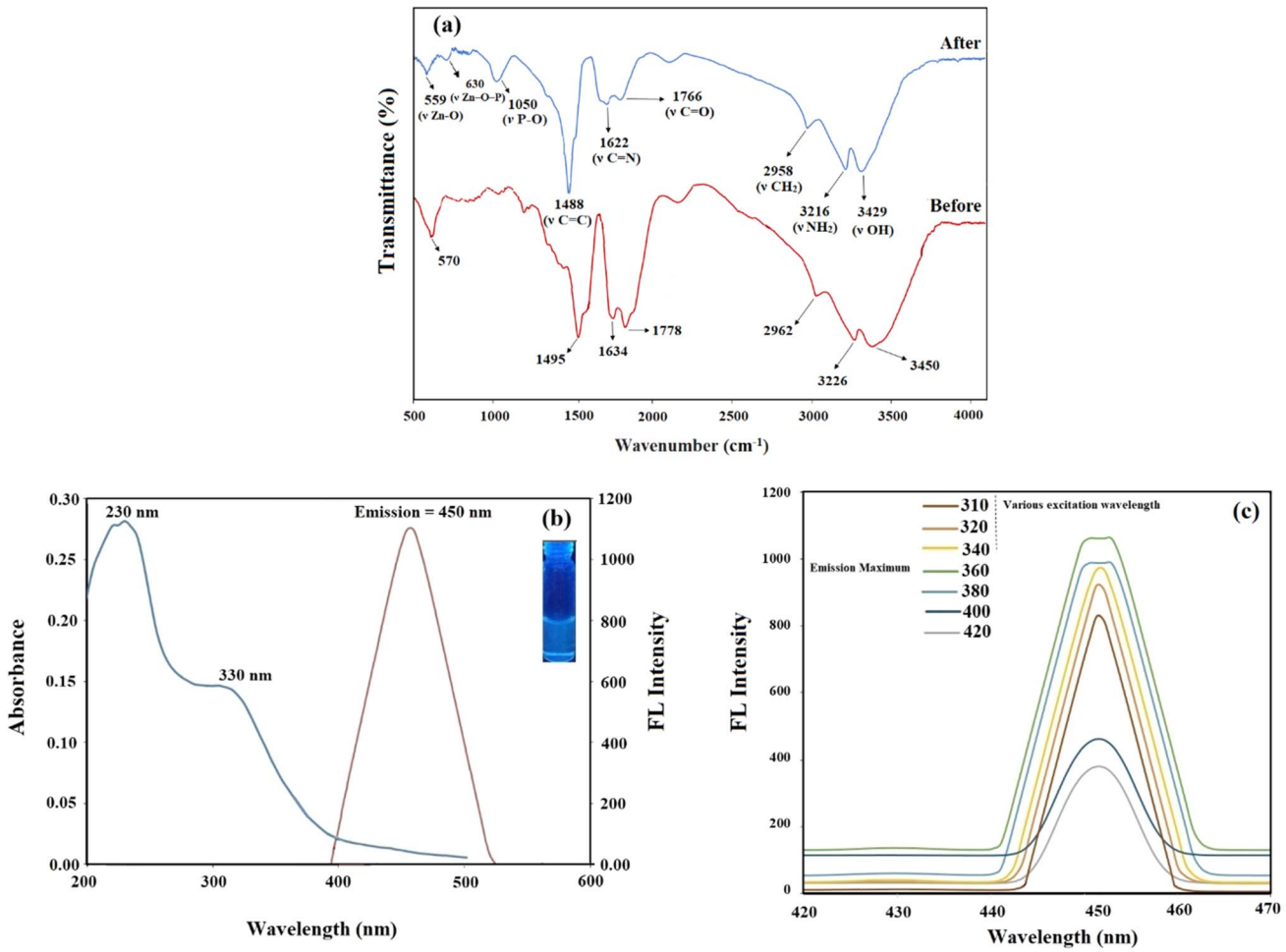

Fig. 1 (a) FT-IR spectrum of Zn-N-CDs before and after adsorption (b) the UV-vis spectrum (blue curve) and fluorescence emission intensity spectrum (red curve) at $\lambda_{ex} = 360$ nm of Zn-N-CDs whereas inset showing the photograph of Zn-N-CDs solution under UV light, (c) fluorescence intensities of Zn-N-CDs at different excitation wavelength (310–420 nm).

shows a broad peak at 3450 cm^{-1}, which is attributed to the stretching vibration of the hydroxyl group.[25] The peaks can be observed at 3226 cm^{-1} and 2962 cm^{-1} indicating the asymmetric stretching vibration of the NH_2 group and asymmetric stretching vibrations of the CH_2 group, respectively.[26] The presence of hydrophilic groups in the structure of Zn-N-CDs, such as ν(O–H) and ν(N–H), can result in great solubility in polar solvents.[27] The absorption peaks at 1778, 1634, and 1495 cm^{-1} are related to the stretching vibration of the C=O, C=N, and C=C bonds.[28] Additionally, a band at 570 cm^{-1} is attributed to the metal-carbon dot stretching vibration (ν(Zn–O)).[28] These results confirm the presence of functional groups such as –OH, –NH, C–H, C=O, C=N, C=C, and Zn–O in N-CDs.

After the PO_4^{3-} adsorption, there was a shift towards lower wavelengths (Fig. 1a), which could have been caused by a chemical interaction resulting in the formation of complexes containing acidic oxygen and dehydration.[29] Adsorption of PO_4^{3-} significantly reduced the intensity on Zn–O stretching vibration, indicating the interaction between PO_4^{3-} and the surface functional groups of Zn-N-CDs. Additionally, it was observed that a new band emerged at 1050 cm^{-1}, which was attributed to the presence of new C–O–P bonds in the structure of Zn-N-CDs.[11] Additionally, the peak at 630 cm^{-1} supported the Zn–O–P stretching vibration and demonstrated that P and the Zn-doped carbon dots can interact during of the adsorption process.[30]

3.1.2 The optical properties of Zn-N-CDs. The optical properties of Zn-N-CDs were investigated by UV-vis and fluorescence spectroscopy analyses (Fig. 1b and c). The UV-vis spectra showed a major peak at 230 nm and a weak shoulder near 330 nm. These peaks correspond to the $\pi \rightarrow \pi^*$ transitions of electrons in the conjugated C=C band and the $n \rightarrow \pi^*$ transitions of C=N, and C=O bonds in Zn-N-CDs.[27,31] Furthermore, the fluorescence emission spectra showed the maximum emission intensity at 450 nm after excitation at 360 nm (Fig. 1b). Optical images of the aqueous Zn-N-CDs solution (inset of Fig. 1b) show the pale blue under 365 nm of UV-light.

Fig. 1c depicts the fluorescence emission spectra of Zn-N-CDs at various excitation wavelengths (310–420 nm). The difference in the excitation wavelength only resulted in a rapid decline in the intensity of the emission wavelength, with no

alteration in peak position. Hence, the findings indicate that the excitation wavelength influences the fluorescence intensity of the Zn-N-CDs. Also, this observation demonstrates the remarkably uniform surface structure and narrow size distribution of Zn-N-CDs.[32] In addition, the maximum fluorescence intensity was obtained at λ_{ex} = 360 nm. Furthermore, an assessment of the quantum yield (QY) of the Zn-N-CDs indicated that it exhibited a significantly high QY. The QY of Zn-N-CDs using quinine sulfate (QY = 0.54) as standard was 47.54% at λ_{ex} = 360 nm. Details about this investigation are listed in Table S1 on ESI.† The quantum yield (QY) achieved for the Zn-N-CDs is deemed satisfactory for analytical applications.

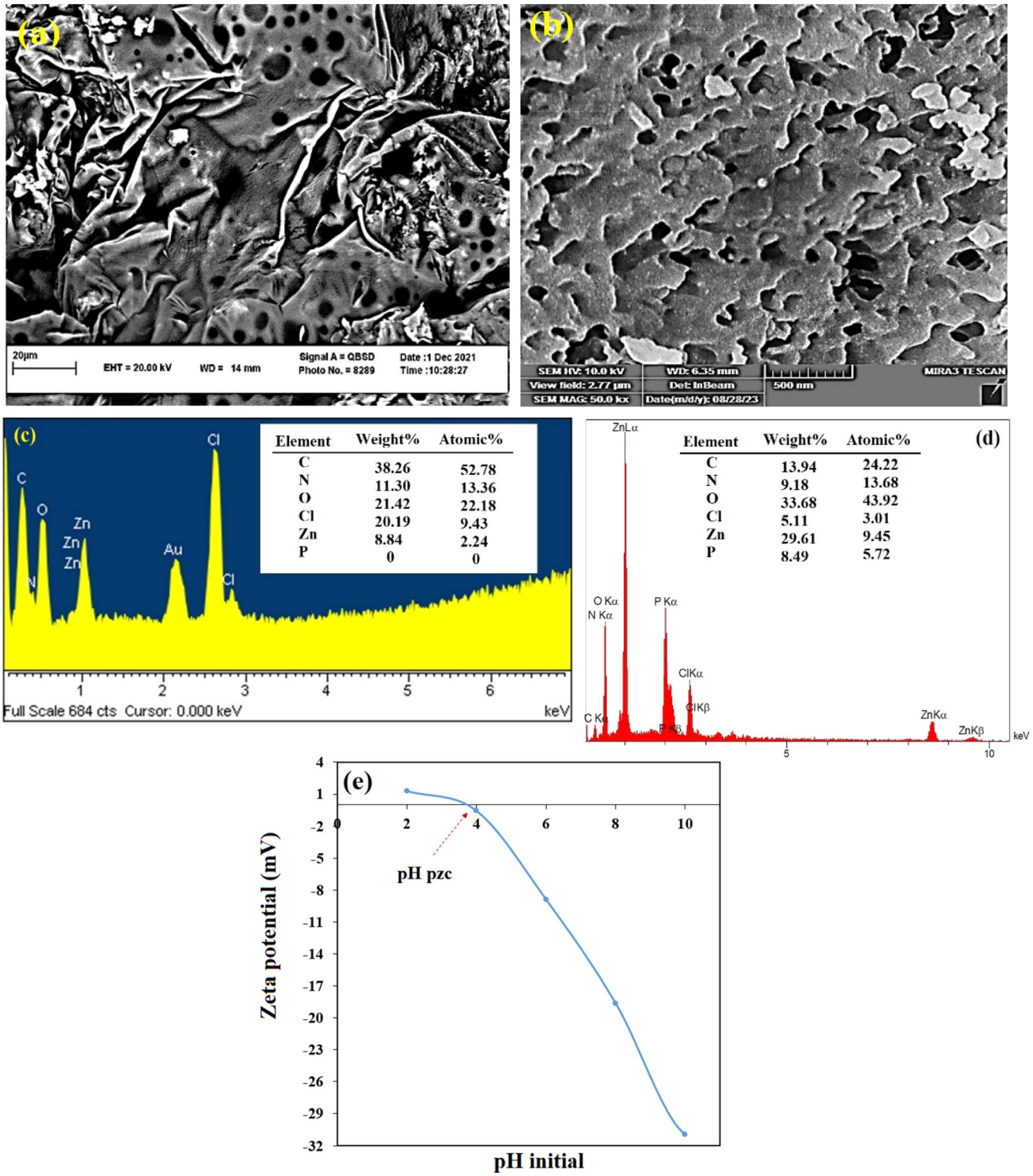

Fig. 2 FESEM of Zn-N-CDs (a) before and (b) after adsorption of PO_4^{3-} (500 mg L^{-1}), elemental composition of Zn-N-CDs (c) before and (d) after adsorption of PO_4^{3-}, and (e) zeta potential of Zn-N-CDs at different pHs.

3.1.3 FESEM/EDS & TEM. FESEM and TEM techniques were used to confirm the morphology and structure of Zn-N-CDs. FESEM images revealed the amorphous nature of carbon with many pores (Fig. 2a). A large number of elliptical pores were observed on the surface of Zn-N-CDs. The FESEM image in Fig. 2b depicts the morphology of the Zn-N-CDs after the adsorption of phosphate ions. The surface of the Zn-N-CDs appears rougher and potentially contaminated, which can be attributed to the adsorption of the phosphate ions onto the adsorbent's surface. Additionally, the surface morphology of the adsorbent after the adsorption process shows smaller pores compared to the pre-adsorption state. This indicates that the adsorbate has been deposited on the surface of the adsorbent.[29]

The TEM images of Zn-N-CDs showed spherical particles that were uniformly dispersed without obvious aggregation (Fig. 2S†).[33] The diameter of the Zn-N-CDs varied between 4 and 5 nm, and an average diameter of 4.3 nm was determined using the particle size distribution plot and fitting the histogram to a Gaussian model (Fig. 2S†). Also, the particle size of Zn-N-CDs was determined to be about 17 nm by using DLS measurement (Fig. 3S†). The hydrodynamic diameter of particles in a solvent is typically larger than the particle size measured in a vacuum. The presence of a hydration layer on the Zn-N-CDs surface in an aqueous solution leads to an increase in particle size.[34]

The results of electron disperse X-ray (EDS) analysis before and after adsorption of PO_4^{3-} (500 mg L^{-1}) are shown in Fig. 2c and d. The results depict that there were decreases in carbon (38.26–13.94 wt%); chlorine (20.19–5.11 wt%) and increases in oxygen (21.42–33.68 wt%) and zinc (8.84–29.61 wt%) contents. After the PO_4^{3-} adsorption, the reduction of the chloride content occurred due to the anions exchange between PO_4^{3-} and chloride from the surface of Zn-N-CDs.[11] The increase in the weight percentage of zinc (from 8.84 to 29.61 wt%) after PO_4^{3-} adsorption suggests that some of the zinc ions in the aqueous solution may have been adsorbed onto the surface of the carbon dots along with the PO_4^{3-}, which will be discuss in the following sections. Furthermore, the presence of P elements (8.49 wt%) and the increase in oxygen percentage (from 21.42 to 33.68 wt%) indicate the adsorption of PO_4^{3-} ions onto the absorbent surface.

3.1.4 The DLS particle size and zeta potential analyzer. Fig. 2e illustrates the zeta potential of Zn-N-CDs at various pH levels. The Zn-N-CDs had a negative surface charge at pH 4–10 due to the existence of carboxyl and/or hydroxyl functional groups on the surface of Zn-N-CDs. The sensitivity of zeta potential to alterations in pH and ionic strength during dilution has been observed.[35] At alkaline pH values higher than pH 7, the zeta potential remained highly negative, indicating the presence of stable anions. However, with the decrease of pH below 7 (in the acidic region), the zeta potential gradually decrease until it reached zero at pH ≈ 4, also known as the zero point charge. This phenomenon occurs when the potential shifts from negative to positive (or *vice versa*).[22] At pH 2, the zeta potential became positive, indicating the protonation of surface functional groups of the Zn-N-CDs.

3.1.5 BET analysis. The surface areas of the carbon dots were determined using the N_2 absorption–desorption method in the low-pressure range, which involved the application of the Brunauer–Emmett–Teller (BET) model. Additionally, the pore size distribution was investigated using the Barrett–Joyner–Halenda (BJH) method (Fig. 3b).

According to the BJH analysis, the carbon dots exhibited a surface area of 107.17 $m^2\ g^{-1}$ and a total pore volume of 0.18 $cm^3\ g^{-1}$. The average pore size was observed to be 6.76 nm. As shown in Fig. 3a, the adsorption–desorption isotherms can be classified as type IV according to the Brunauer–Deming–Deming–Teller (BDDT) classification, with a prominent hysteresis loop at medium pressure (Fig. 3a). This suggests the presence of a mesoporous structure within the carbon dots.[36]

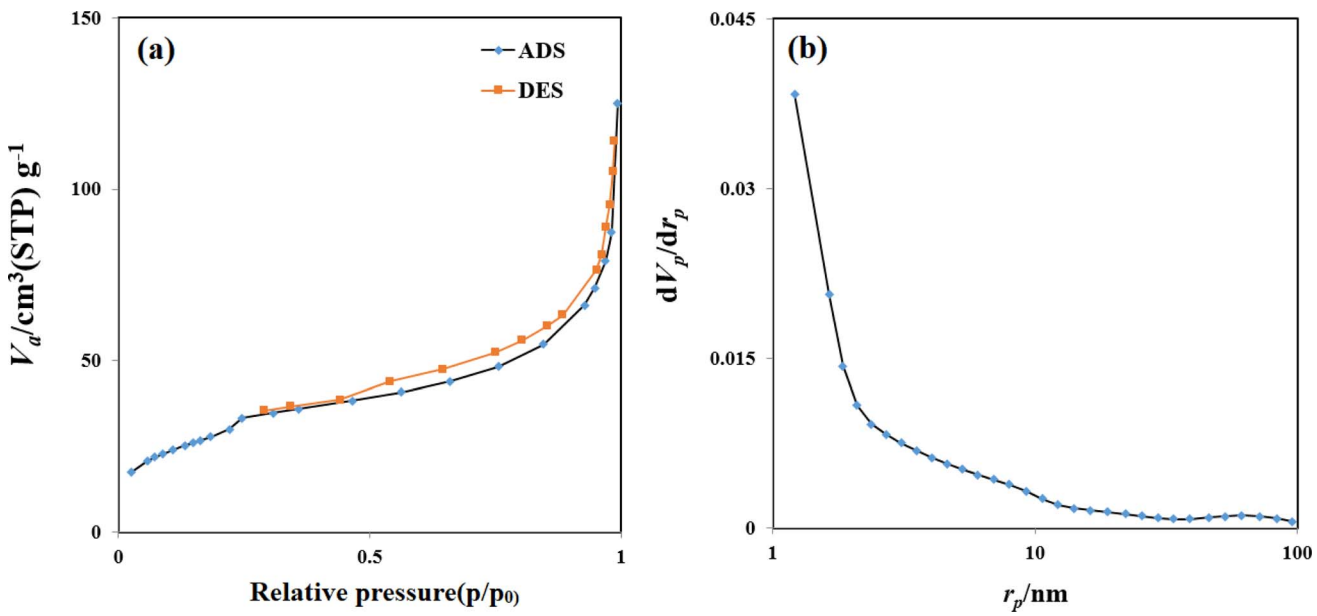

Fig. 3 (a) Adsorption–desorption isotherms and (b) pore size distribution curves of the Zn-N-CDs.

The high surface area and mesopores in the Zn-N-CDs provide ample adsorption sites and efficient mass transfer, respectively, which are crucial for effectively removing PO_4^{3-} from aqueous environments. The mesoporous structure facilitates the diffusion of phosphate-containing species into the porous network, while the large surface area enhances the adsorption capacity of the Zn-N-CDs.

3.2 Kinetic and thermodynamic studies of PO_4^{3-} adsorption

The effect of contact time and temperature on PO_4^{3-} adsorption using Zn-N-CDs was evaluated (Fig. 4a). PO_4^{3-} underwent a fast reaction by Zn-N-CDs and the amount of PO_4^{3-} adsorption at temperatures 21, 35, and 45 °C were 110.62, 98.02, and 73.2 mg g^{-1}, respectively. In fact, the process achieved equilibrium in within 5 minutes, and no additional substantial adsorption was found. This fast reaction could be attributed to high surface area and the structure of Zn-N-CDs. Carbon dots contain numerous active adsorption sites, as indicated by the FT-IR spectrum (Fig. 1a). Furthermore, by doping Zn^{2+} onto the carbon dots particles and creating a new composite, the number of adsorption sites capable of binding with PO_4^{3} increased.[11] Hence, PO_4^{3-} adsorption on Zn-N-CDs exhibits a high reaction rates. Various interactions such as physical adsorption, anion exchange, precipitation, and complexation may account for the rapid adsorption of PO_4^{3-},[10,11,37] as will be explained later.

The experimental results were described by three noticeable kinetic models (Table 1). A key element in establishing which kinetic model is suitable for explaining experimental results is the regression coefficient (R^2).[5] As a result, the high regression coefficient (0.999) pseudo-second-order model was better suited to describe data. At 21, 35, and 45 °C, the regression coefficients of the pseudo-second-order model were significantly higher than those of the pseudo-first-order and intra-particle diffusion kinetic models. This strong match indicates that chemisorption interactions which entail the creation of chemical bonds between the adsorbate and the adsorbent are primarily responsible for the PO_4^{3-} adsorption onto Zn-N-CDs.[8,9] Furthermore, comparing the adsorption capacity predicted by the kinetic models ($q_{e.cal}$) with the adsorption capacity determined from experimental data ($q_{e.exp}$) is also important.[5] Table 1 shows that the $q_{e.cal}$ values for the pseudo-second-order at temperatures 21, 35, and 45 °C are 112.36, 100, and 79.37 mg g^{-1}, respectively, which are much closer to $q_{e.exp}$ values obtained from experimental data. In addition, at 21 °C, 35 °C, and 45 °C, the pseudo-second-order kinetic model's rate constants (K values) were found to be 0.038, 0.033, and 0.023, respectively. The pseudo-second-order model's lower K values emphasize the relative speed of the adsorption process in addition to demonstrating the model's adequacy in explaining the experimental results.[8] Therefore, the high regression coefficient, adsorption capacity ($q_{e.cal}$), and lower K values of the pseudo-second-order

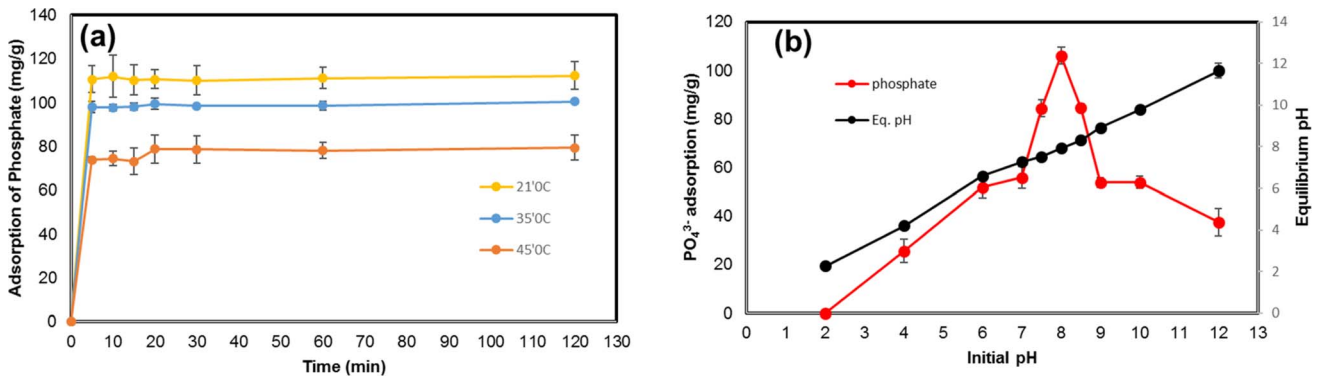

Fig. 4 (a) The effect of contact time and temperature on PO_4^{3-} adsorption ([Zn-N-CDs] = 3 g L^{-1}, ionic strength 10 mM KCl, [PO_4^{3-}] = 500 mg L^{-1}, without adjusting pH, shaking time) (b) the effect of pH on PO_4^{3-} adsorption ([Zn-N-CDs] = 3 g L^{-1}, ionic strength 10 mM KCl, [PO_4^{3-}] = 500 mg L^{-1}, shaking time = 5 min, 21 °C).

Table 1 Kinetic and thermodynamic parameters of PO_4^{3-} adsorption onto Zn-N-CDs

	Pseudo-first-order				Pseudo-second-order			Intraparticle diffusion		
T (°C)	$q_{e.exp}$	$q_{e.cal}$ (mg g^{-1})	K_1 (min^{-1})	R^2	$q_{e.cal}$ (mg g^{-1})	K_2 (g min^{-1} min^{-1})	R^2	C	K_p (mg g^{-1} $min^{-1/2}$)	R^2
21	110.62	5.37	−0.0003	0.1615	112.36	0.038	0.999	65.553	6.6668	0.3305
35	98.02	7.09	−0.0003	0.2271	100	0.033	0.999	57.902	6.0064	0.3393
45	79.46	10.84	−0.0004	0.4255	79.37	0.023	0.999	43.45	4.9799	0.3841
T (K)	$\Delta G°$ (KJ mol^{-1})				$\Delta H°$ (KJ mol^{-1})			$\Delta S°$ (J mol^{-1} K^{-1})		
294	−16.16				0.163			54.14		
308	−15.87									
318	−14.8									

indicate that the PO_4^{3-} adsorption by Zn-N-CDs follows the pseudo-second-order kinetic equation. Comparable results for green-synthesized iron nanoparticles,[8] Zinc Oxide Betaine-Modified Biochar Nanocomposites (ZnOBBNC),[1] halloysite nanotubes (HNTs),[3] and Mg-Al-LDH[11] have been documented in the literature.

Table 1 shows the thermodynamic parameters of PO_4^{3-} adsorption onto Zn-N-CDs. The negative values of $\Delta G°$, at 21 °C, 35 °C, and 45 °C specify that the PO_4^{3-} adsorption onto Zn-N-CDs is a spontaneous process. This means that the process may occur without the need for external energy input, emphasizing an essential aspect of efficient adsorption processes. As the temperature increased, the $\Delta G°$ values decreased, indicating that higher temperatures were less favorable for adsorption. The endothermic feature of adsorption was confirmed by the positive result of $\Delta H°$ (0.163). The increase in randomness at the solid/solution interface during the adsorption of PO_4^{3-} onto Zn-N-CDs is indicated by the positive value of $\Delta S°$ (54.14).[8,11,38,39] As is common for adsorption events where new configurations between adsorbate and adsorbent are produced, these results suggest that the adsorption process is not only energy-dependent (endothermic) but also leads to a more disordered state at the interface.[1,8,11] These finding also align with the adsorption of PO_4^{3-} onto other adsorbents, such as Mg-Al-LDH,[11] IONP,[38] FeMg2Mn-LDH,[39] and green-synthesized iron nanoparticles.[8]

3.3 Effect of pH on PO_4^{3-} adsorption and possible mechanisms

A variation of pH not only could change the speciation of ions in the solution but also can affect the surface chemistry of the adsorbent. The evaluation of this phenomenon can illustrate the absorbent behavior in the natural environment. For this reason, the effect of pH on PO_4^{3-} adsorption onto Zn-N-CDs is investigated and depicted in Fig. 4b. At acidic pH ($\approx$2) no significant adsorption of PO_4^{3-} was detected. Moreover, by increasing pH, the PO_4^{3-} adsorption dramatically increased and the maximum adsorption was reached 105.96 mg g^{-1} at pH 8. After pH 8, the process of PO_4^{3-} adsorption decreased drastically. For explanation of reactions between adsorbent and adsorbate, some factors should be noted, including: (1) physicochemical structure of Zn-N-CDs, (2) speciation of PO_4^{3-} ions in solution, and (3) the role of zinc ions in the reaction.

As FT-IR spectrum (see Fig. 1a), Zn-N-CDs contain numerous active adsorption sites such as –OH, $-NH_2$, and zinc hydroxide. These functional groups have a decisive role in PO_4^{3-} adsorption.[1,4,10,11] In acidic pH, the functional groups can be protonated, which helps to retain PO_4^{3-} electrostatically.[1] However, the surface zeta potential of the adsorbent at different pH (Fig. 2e) depicts that the Zn-N-CDs contain negligible surface positive charge at pH 2 and at pH 4 (also known as pHpzc), and the net surface charge is almost neutral. Therefore, the capability of the adsorbent to adsorb PO_4^{3-} electrostatically, at highly acidic pH, is relatively low and the Zn-N-CDs, in a wide variety of pH, including negative surface charge. It means that increasing pH accelerates the deprotonation of the functional groups of the adsorbent, and the net surface charge is negative. For this reason, electrostatic attraction might not be the main mechanism to remove PO_4^{3-} from the solution. On the other hand, by increasing pH and deprotonation of the surface functional groups, it is expected that the electrostatic repulsion force between PO_4^{3-} and Zn-N-CDs increases, which can reduce the adsorption of PO_4^{3-} on the negative surface charge of particles. However, by increasing pH, the amount of adsorption dramatically increased. Therefore, to explain this occurrence, other possible interactions between adsorbent and adsorbate should be mentioned.

Accordingly, the distribution of PO_4^{3-} species in a solution as a function of pH is crucial (eqn (11)–(13)).[3,7] At pH = 2, the dominant species is H_3PO_4. Meanwhile, the H_3PO_4 is uncharged, the low adsorption capacity at highly acidic pH could attributed to this phenomenon.[1,9] By increasing pH, the concentration of $H_2PO_4^-$ and HPO_4^{2-} gradually increase. Since, the net surface charge of Zn-N-CDs is negative, PO_4^{3-} adsorption mainly occurs through chemisorption interactions,[1,10,40] which will be discussed in the following lines.

$$H_3PO_4 \leftrightarrow H_2PO_4^- + H^+ \mathrm{p}K_{a1} = 2.15 \quad (11)$$

$$H_2PO_4^- \leftrightarrow HPO_4^{2-} + H^+ \mathrm{p}K_{a2} = 7.2 \quad (12)$$

$$HPO_4^{2-} \leftrightarrow PO_4^{3-} + H^+ \mathrm{p}K_{a3} = 12.35 \quad (13)$$

Generally, metal oxide (hydroxides) have high affinity to adsorb PO_4^{3-} ions.[10] PO_4^{3-} could react with zinc hydroxides through ligand exchange. In addition, active sites of zinc hydroxides and PO_4^{3-} ions act as Lewis base and Lewis acid, respectively. As a result of these reactions, Zn–O form bonds with oxygen ions of PO_4^{3-}. Consequently, monodentate-mononuclear (MM), bidentate-mononuclear (BM), and bidentate-binuclear (BB) inner-sphere complexes could be formed (eqn (14)–(16)).[10,11] The fact that PO_4^{3-} adsorption increases with increasing pH might therefore be due in part to these processes. Additionally, inner–sphere complex interactions could raise the equilibrium pH by releasing OH ions into the solution.[2,11] However, based on Fig. 4b, the equilibrium pH remained steady during the adsorption process. This discrepancy might be explained through the role of zinc and PO_4^{3-} ions in the solution. Exploring these roles could unravel the main mechanisms of PO_4^{3-} adsorption.

$$\equiv Zn\text{–}OH + H_2PO_4^- \leftrightarrow \equiv Zn\text{–}H_2PO_4^- + OH^- \text{ (MM)} \quad (14)$$

$$\equiv Zn\text{–}(OH)_2 + HPO_4^{2-} \leftrightarrow \equiv Zn\text{–}HPO_4 + 2OH^- \text{ (BM)} \quad (15)$$

$$(\equiv Zn)_2\text{–}OH + HPO_4^{2-} \rightarrow (\equiv Zn)_2\text{–}HPO_4 + OH^- \text{ (BB)} \quad (16)$$

Most likely, a portion of the zinc cations might release into the solution from the carbon dots structure. The EDS spectrum (see Fig. 2c and d) also confirmed that the percentage of zinc ions in the solution, during the adsorption of PO_4^{3-}, was increased. Free zinc cations are unstable in the solution, which are quickly surrounded by water molecules, resulting in the formation of water–zinc complexes. Proton ions generated by

these processes could buffer the solution (eqn (17) and (18)).[41] On the other hand, dissociation of PO_4^{3-} ions, due to increasing pH, might help to buffer the system.[7]

$$[Zn(H_2O)_6]^{2+} + H_2O \leftrightarrow Zn(OH)_{aq}^{+} + H^+ \quad (17)$$

$$Zn(OH)_{aq}^{+} + H_2O \leftrightarrow Zn(OH)_{2(aq)} + H^+ \quad (18)$$

By improving pH from 2 to 8, the concentration of zinc species in the solution such as $Zn(OH)^+$ and $Zn(OH)_2$ gradually increase.[41] The adsorbed PO_4^{3-} on the Zn-N-CDs surface, might act as a new adsorption site for zinc hydroxides in the solution forming a surface precipitate. Meanwhile, the zinc ion that has been adsorbed could play as a sorption site for the PO_4^{3-} which is still in the solution.[10,11] As a result of these reactions (anion exchange, complexation, and precipitation), hopeite ($Zn_3(PO_4)_2 \cdot 4H_2O$) can develop on the surface of Zn-N-CDs structure.[10] In addition, there is the possibility of ion exchange between PO_4^{3-} in the solution and chloride ions that are adsorbed onto the Zn-N-CDs (eqn (19)) [5]. These interactions and possibilities indicate that the adsorption of PO_4^{3-} using the synthesized particles might occurred through multi-layer adsorption, which will be discussed in the Sections 3–6. Furthermore, in another study, when Zn-Mg-Al-LDH was utilized to remove PO_4^{3}, zinc ions played a crucial role in the buffering of a system and multi-layer adsorption of PO_4^{3-}.

$$\equiv 2CD\text{–}Zn\text{–}OH + ZnCl_2 + 3H_2PO_4^- \rightarrow \equiv 3CD\text{–}Zn\text{–}H_2PO_4 + 2Cl^- + 2OH^- \quad (19)$$

The results of FT-IR spectrum, FESEM, and EDS spectrum confirmed these potential mechanisms. Moreover, PO_4^{3-} can react with monovalent and divalent cations in the solution and form precipitation on the surface of Zn-N-CDs, which will be discussed in the following section. After reaching pH 8, the amount of PO_4^{3-} adsorption drastically decreased. Indeed, in basic pH, the functional groups on the surface of Zn-N-CDs are dissociated, leading to an increase in the negative charge on the surface. As a result, the adsorption of PO_4^{3-} is reduced due to the enhanced repulsion between the negatively charged surface of Zn-N-CDs and the phosphate ions.[1,9] Furthermore, OH^- ions in the basic pH, compete with PO_4^{3-} ions on active adsorption sites.[9] Other research also confirmed this possibility. When HA520E-Fe (hybrid polymeric anion exchanger impregnated with hydrated Fe(III) oxide) was used to remove PO_4^{3-}, by increasing pH, the adsorption process also increased; however, after pH 7 the efficiency of PO_4^{3-} adsorption drastically decreased.[7] By explaining the above phenomena and clarifying the interactions, the probable mechanisms of PO_4^{3-} adsorption on Zn-N-CDs are illustrated in Fig. 5.

3.4 Effect of monovalent and divalent cations on PO_4^{3-} adsorption

The background solution, by affecting the thickness of the electrical double layer of an adsorbent and increase/decrease of surface charge, has a decisive role in interactions between adsorbent and adsorbate. The evaluation of these situations could unravel the behavior of the adsorbent in the natural

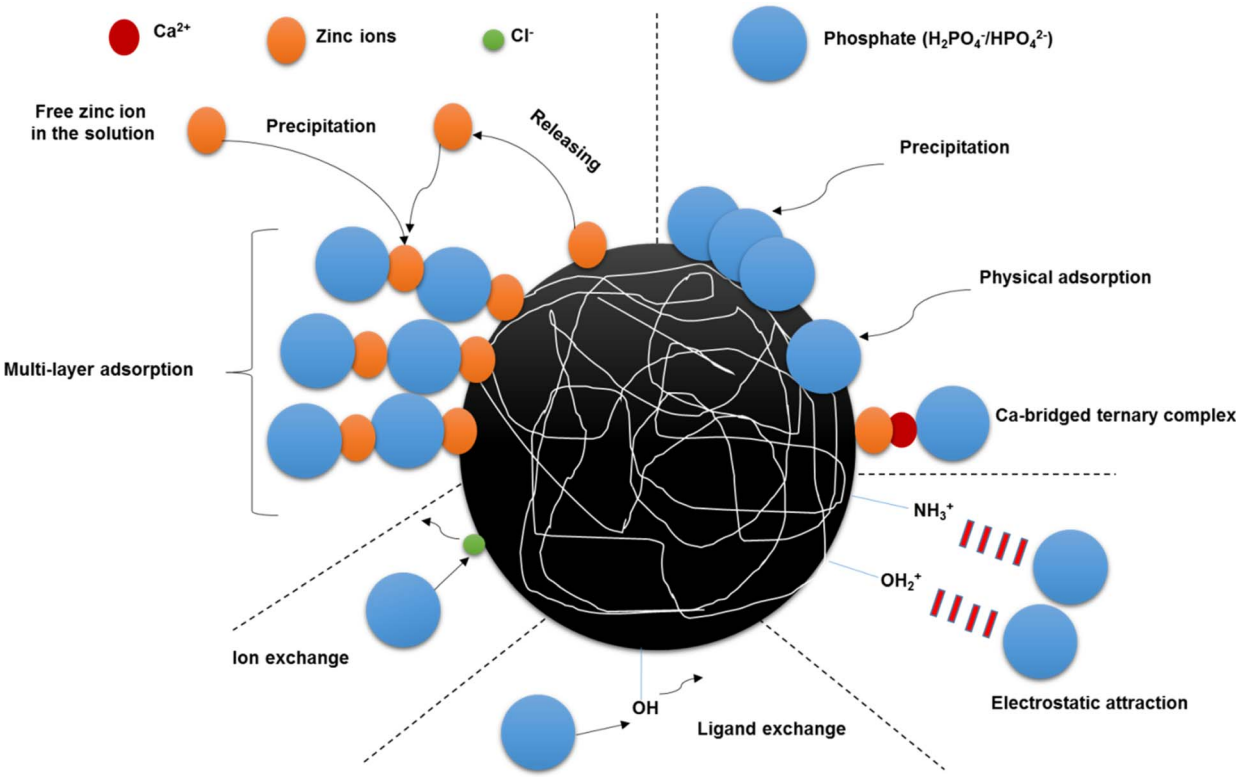

Fig. 5 The possible mechanisms of PO_4^{3-} adsorption using Zn-N-CDs.

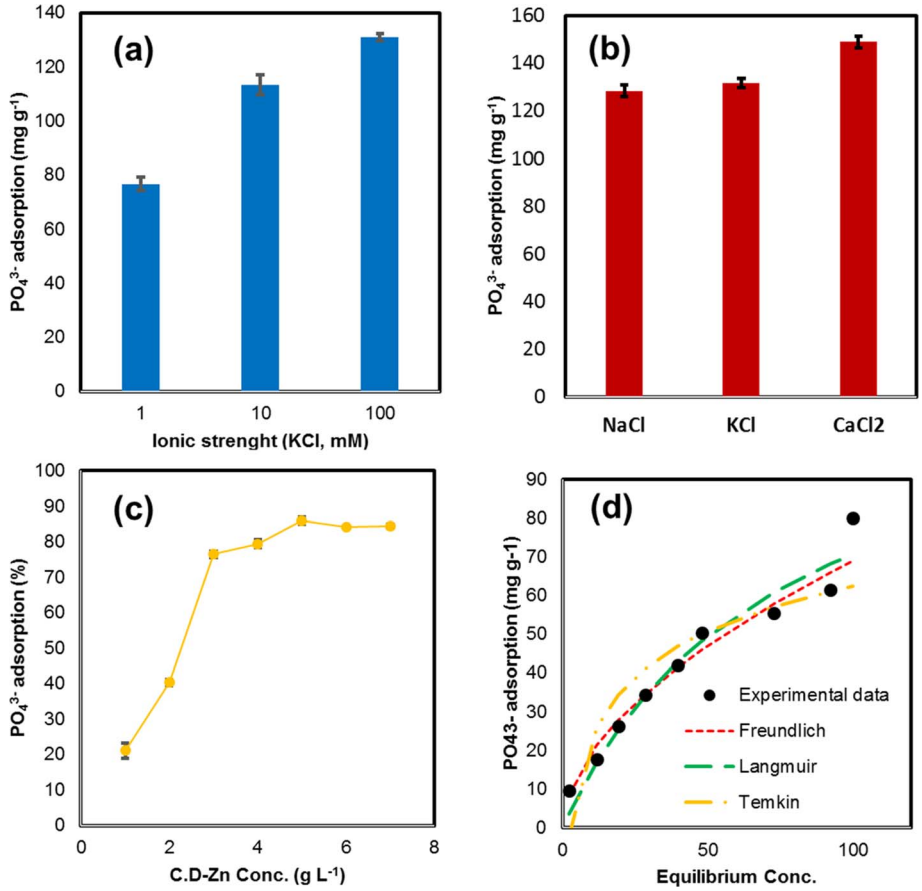

Fig. 6 (a) The effect of KCl concentration as an ionic strength on PO_4^{3-} adsorption, (b) the effect of different background solutions with same concentration (100 mM) on PO_4^{3-} adsorption ([Zn-N-CDs] = 3 g L^{-1}, [PO_4^{3-}] = 500 mg L^{-1}, shaking time = 5 min, 21 °C), (c) the effect of adsorbent dosage on PO_4^{3-} adsorption ([Zn-N-CDs] = 1–7 g L^{-1}, [PO_4^{3-}] = 500 mg L^{-1}, ionic strength 100 mM KCl, shaking time = 5 min, 21 °C), (d) equilibrium isotherms of PO_4^{3-} adsorption on Zn-N-CDs ([Zn-N-CDs] = 5 g L^{-1}, [PO_4^{3-}] = 50–500 mg L^{-1}, I = 100 mM KCl, shaking time = 5 min, 21 °C).

environment. For this reason, PO_4^{3-} adsorption was investigated in a background solution of 10–100 mM KCl (Fig. 6a). The results from the experiments indicate that the adsorption increases by increasing electrolyte concentration and high PO_4^{3-} adsorption capacity (130.93 mg g^{-1}) occurred at 100 mM KCl concentration. The presence of K^+ ions in the reaction could change the electric potential at the interface of Zn-N-CDs. Indeed, through increasing electrolyte concentration and adsorption of K^+ ions on the surface of Zn-N-CDs, the thickness of electrical double layer (EDL) decreases.[40,42,43] Therefore, the electrostatic repulsion between PO_4^{3-} ions and the charged surface decline, which favors adsorption and formation of inner-sphere complexations.[40,42,43] Furthermore, K^+ ions that adsorbed on the surface of Zn-N-CDs, can act as a bridge (between PO_4^{3-} and the charged surface) to enhance the adsorption process through outer-sphere complexation.[40,43] Also, in previous research, by increasing the concentration of KNO_3, as a background solution, PO_4^{3-} adsorption increased.[40]

In addition, the PO_4^{3-} adsorption capacity on Zn-N-CDs was evaluated in different background solution (concentration = 100 mM) including NaCl, KCl and $CaCl_2$ salts (Fig. 6b). The results show that the PO_4^{3-} adsorption in the presence of $CaCl_2$ > KCl > NaCl. The adsorption capacity of PO_4^{3-} in the $CaCl_2$, KCl, and NaCl were acquired 148.89, 131.71, and 128.46 mg g^{-1}, respectively. The surface charge density of the cations could explain this occurrence, which $Na^+ > K^+ > Ca^{2+}$ has a surface charge density, respectively. Therefore, when these cations expose into the solution, they are surrounding with water molecules and from H_2O-cations complexes. Any cation that has a lower surface charge density has a relatively smaller hydration radius. This means that the cation with a smaller hydration radius can better approach the surface of the adsorbent and neutralize the negative surface charge of the particles. The neutralization of the negative charge on the surface means the decline of the thickness of the electric double layer (EDL) of the absorbent, and also the reduction of the electrostatic repulsion force between the absorbent and the adsorbate.[42,44] Ca^{2+} compared to K^+ and Na^+ has lower hydration radius, which at the solid–solution interface could decrease surface negative charge and electrostatic repulsion forces. Therefore, PO_4^{3-} ions can easily approach the surface of the adsorbent to form chemical adsorption.[44] This reaction was confirmed in a previous study by Zong *et al.*[2] who investigated PO_4^{3-} adsorption onto SCBC-La. They reported that increasing NaCl

concentration as a background solution did not increase the adsorption capacity of PO_4^{3-}. However, in another study, when Ca^{2+} ions were chosen as a background solution, the PO_4^{3-} adsorption improved.[42]

As mentioned before, by decreasing the electrical double layer and approaching PO_4^{3-} to the charged surface, the adsorption capacity increased. This issue leads to cascades of reactions including electrostatic adsorption, precipitation, and complexation.[44] Based on literature, metal oxyhydroxides have high affinity for adsorbing Ca^{2+}.[42] The adsorption of Ca^{2+} on charged surface could stimulate the adsorption of PO_4^{3-} and *vice versa*.[42] The adsorbed Ca^{2+} by producing surface positive charge increase the electrostatic adsorption of PO_4^{3-}. Furthermore, the Mendez & Hiemstra[44] argued that ternary complex formation could occur on the surface of metal oxyhydroxides. Indeed, Ca^{2+} act as a bridge and cation-bridged ternary complex (M–Ca–PO_4) could develop on the surface. On the other hand, by increasing pH, the PO_4^{3-} surface speciation can change from monodentate-protonated to bidentate-deprotonated leading to increase the surface negative charge.[42,44] Consequently, PO_4^{3-} act as a bridge and PO_4-bridged ternary complex could form (M-PO_4-Ca).[44] Furthermore, interaction of Ca-PO_4 increase with rising pH and solid phase can precipitate as octa-Ca-PO_4 ($Ca_4H(PO_4)_3\cdot 2.5H_2O$), β-tri-Ca-$PO_4$ ($Ca_3(PO_4)_2$), and hydroxyapatite (HPA) on the surface of Zn-N-CDs.[44] Additionally, some researches claimed that both ions, Ca^{2+} and PO_4^{3-}, are bonded monodentately to the charged surface, but there is also an additional chemical reaction (lateral interaction) between the adsorbed cations and anions.[44,45]

3.5 Effect of adsorbent dosage

The optimal level of Zn-N-CDs dosage for PO_4^{3-} adsorption is illustrated in Fig. 6c. The experimental results indicate that by increasing the adsorbent dosage, due to enhancement specific surface area and active adsorption sites, the PO_4^{3-} adsorption increased, and by using 5 g L^{-1} of adsorbent, 85.81% of initial PO_4^{3-} concentration (500 mg L^{-1}) was adsorbed (maximum adsorption). However, the adsorption capacity at higher concentrations of Zn-N-CDs dosage remains steady. This behavior is due to the large number of Zn-N-CDs active sites compared to the PO_4^{3-} concentration. In addition, this may be due to the PO_4^{3-} mass transfer resistance at high adsorbent dosages from the bulk liquid to solid surface sites.[1,43] Acquiring the optimal dosage of adsorbent could help avoid over-consumption of Zn-N-CDs and increase the adsorbent efficiency in aquatic and terrestrial environments.[46] Therefore, 5 g L^{-1} of Zn-N-CDs was chosen as the optimal dosage for further experiments.

3.6 Adsorption isotherms

Adsorption isotherm models can explain the interactions between adsorbent and adsorbate. Therefore, in order to describe and clarify the adsorption mechanism, the isotherm models such as Freundlich, Langmuir, and Temkin were applied in different initial PO_4^{3-} concentrations (50–500 mg L^{-1}). The Freundlich model indicates that the adsorption process is multi-layer, which happens on heterogeneous sites. This model deduces that there are non-homogeneous affinities and heat distribution of adsorption toward the heterogeneous surface.[9,43,47] Unlike the Freundlich model, the Langmuir isotherm model has some assumptions, monolayer adsorption occurs on homogenous sites, and adsorption energy is constant. In addition, in this model, no lateral interaction happens between adsorbed molecules.[9,43,47] The Temkin isotherm model also presumes multi-layer adsorption; however, it cannot be utilized for very low and high concentration values. Furthermore, the Temkin model proposes that all of the molecules in the layer experience a linear decrease in heat of adsorption.[47] As shown in the experimental data (Fig. 6d), PO_4^{3-} adsorption capacity using Zn-N-CDs increased with increasing initial PO_4^{3-} concentration. The adsorbent indicated the high adsorption capacity under optimal condition. These data depict that the Zn-N-CDs can be used to remove PO_4^{3-} from aquatic solutions, both at low and high concentrations. Based on Langmuir model, the maximum adsorption capacity is 122.417 mg g^{-1}. This value is higher than that of some other adsorbents discussed in Section 3.8.

Based on the data obtained from the isotherm models (Table 2), the experimental data well fitted to the Freundlich model when R^2 is 0.9754, and this value is higher than the R^2 values of the Langmuir ($R^2 = 0.906$) and the Temkin model ($R^2 = 0.8368$). As mentioned above, the Freundlich model suggests that the surface of Zn-N-CDs is heterogeneous and that the adsorption of PO_4^{3-} ions occurs in multiple layers.[43] Additionally, the high value of K_F (5.477) in the Ferundlich model indicates that PO_4^{3-} could easily adsorb onto Zn-N-CDs. Furthermore, the $1/n$ value in the Ferundlich model indicates the adsorption intensity or surface heterogeneity. When $1/n > 1$ and $1/n = 1$, it presumes that the adsorption process is unfavorable and irreversible, respectively.[43,47] However, when $0 < 1/n < 1$ demonstrates that the adsorption process is favorable even at high concentrations of PO_4^{3-}. Constantly, these obtained data specify that the Ferundlich model might clarify the adsorption mechanism. Since this model assumes multilayer adsorption, this assumption can confirm the previously discussed adsorption mechanisms (Section 3.3). As we mentioned before, PO_4^{3-} ions adsorb onto the surface of Zn-N-CDs *via* electrostatic and/or ligand

Table 2 Physicochemical parameters of adsorption isotherms of PO_4^{3-} removal using Zn-N-CDs

Isotherm models								
Freundlich			Langmuir			Temkin		
K_F (mg g^{-1})	$1/n$	R^2	Q_{max} (mg g^{-1})	K_L (L mg^{-1})	R^2	B_T (KJ mol^{-1})	K_T	R^2
5.477	0.550	0.9754	122.417	0.014	0.906	16.999	0.395	0.8368

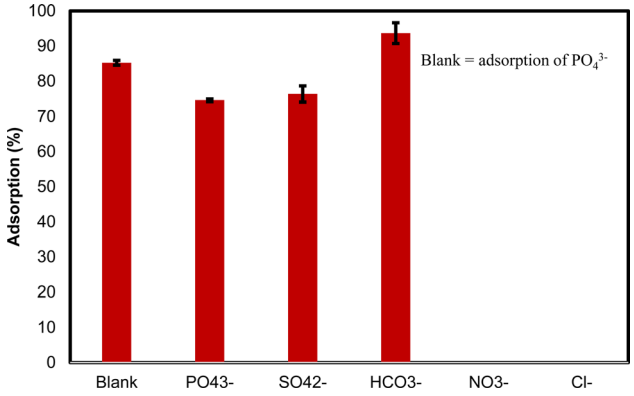

Fig. 7 The effect of competing anions on PO_4^{3-} adsorption ([Zn-N-CDs] = 5 g L^{-1}, [PO_4^{3-}] = [HCO_3^-] = [SO_4^{2-}] = [NO_3^-] = [Cl^-] = 5.2 mM, I = 100 mM KCl, shaking time = 5 min, 21 °C).

exchange. Furthermore, the adsorbed PO_4^{3-} ions could serve as new adsorption sites for zinc ions in the solution. These processes can continue with PO_4^{3-} adsorption by adsorbed zinc ions. These reactions involve multi-layer adsorption procedures, which are consistent with the information provided by the Freundlich model.

3.7 The effect of competing anions

Evaluating the adsorption selectivity of Zn-N-CDs for practical applications is important. Therefore, the effect of coexisting anions including NO_3^-, SO_4^{2-}, HCO_3^-, and Cl^- on PO_4^{3-} adsorption using 5 g L^{-1} of Zn-N-CDs was investigated (Fig. 7). The results showed that 85.22% of initial PO_4^{3-} concentration (5.2 mM) was adsorbed in the blank situation (without competing anions), and in the presence of competing anions (NO_3^-, SO_4^{2-}, HCO_3^-, and Cl^-), this amount reached around 74.58%. Additionally, SO_4^{2-} and HCO_3^- competed with PO_4^{3-} ions on active adsorption sites, resulting in the removal of approximately 76.36% and 93.67% of these anions from the solution, respectively. Furthermore, no significant adsorption of NO_3^- and Cl^- was detected. The data indicates that Zn-N-CDs have a high PO_4^{3-} adsorption capacity in the presence of other anions and the slight decrease in PO_4^{3-} adsorption could be attributed to the competition between PO_4^{3-} and coexisting anions (SO_4^{2-} and HCO_3^-) on the charged surface. Additionally, a recent study evaluated PO_4^{3-} adsorption using LA-CTS-ATP and the researchers reported that SO_4^{2-} had no significant change on PO_4^{3-} adsorption. Furthermore, HCO_3^- drastically decreased the amount of adsorption of PO_4^{3-}.

Moreover, the occupying of active adsorption sites by PO_4^{3-}, SO_4^{2-}, and HCO_3^- through chemisorption, especially PO_4^{3-} ions, could increase the net negative surface charge of the nanoparticles, which leads to the increasing electrostatic force repulsion between adsorbent and adsorbate. While ions such as NO_3^- and Cl^- have electrostatic adsorption, and this kind of adsorption is highly sensitive to the presence of cations, anions, and concentration of media solution, the increase of negative surface charge prevents the adsorption of NO_3^- and Cl^- ions.[5] In addition, in other studies, NO_3^- and Cl^- ions have been reported not to be a good competitor for PO_4^{3-} adsorption due to outer-sphere complexes.[5,11] On the other hand, some literature has reported the presence of coexisting anions, resulting from increasing ionic strength and declining the thickness of electrical double layer, could increase PO_4^{3-} adsorption.[2,5] As mentioned before, PO_4^{3-} can adsorb through monodentate-mononuclear (MM), bidentate-mononuclear (BM), and bidentate-binuclear (BB) inner-sphere complexes. These interactions not only occupy the active adsorption sites but also increase net negative surface charge, which improves the colloidal stability of nanoparticles in an environment. Since the Zn-N-CDs have a high capability to adsorb PO_4^{3-}, even in the presence of competing anions, this phenomenon shows that the Zn-N-CDs are promising nano-adsorbents for application in water and wastewater treatment.

3.8 Comparative studies

Table 3 compared the maximum PO_4^{3-} adsorption capacity using Zn-N-CDs with the other PO_4^{3-}adsorbents previously described in the literature. The adsorption capacity is greater than other sorbents such as Feryhidrate,[43] La-CTS-ATP,[9]

Table 3 Comparison of Zn-N-CDs with other adsorbents

Materials	Maximum adsorption capacity (mg g^{-1})	pH	Equilibrium time (min)	References
ZnOBBNC	265.50	7	15	1
Ferrihydrite	50	7	120	43
La-CTS-ATP	102.9	5	50	9
EL-MNP@Zeolite	59.88	2–8	15	8
Silica and ligand embedded composite	159.12	4	60	4
SCBC-La	58.8	3	1080	2
Ca-BC	13.61	8.5	4320	48
CTAB-modified IONP	18.69	2	90	38
Mn^{2+}/Zn^{2+}/Fe^{3+}/Mg-Al-LDH composite	82.3	7.5	60	11
ZnAlZr4-HT	91	2.3	120	10
Zn-N-CDs	122.417	8	5	Current study

EL-MNP@Zeolite,[8] SCBC-La,[2] Ca-BC,[48] CTAB-modified IONP,[38] $Mn^{2+}/Zn^{2+}/Fe^{3+}$/Mg-Al-LDH composite,[11] and ZnAlZr4-HT.[10] On the other hand, Zn-N-CDs adsorption capacity is lower than ZnOBBNC[1] and silica and ligand embedded composite.[4] However, it appears that the synthesis of Zn-N-CDs is significantly simpler, more affordable, and more environmentally friendly. The maximum PO_4^{3-} adsorption capacity by Zn-N-CDs was obtained in alkaline pH. This indicates the capability of Zn-N-CDs to remove PO_4^{3-} in wide ranges of pH. In addition, the removing of PO_4^{3-} in basic pH reveals that Zn-N-CDs can be used in aquatic and terrestrial environments. Zn-N-CDs also have a more rapid equilibrium time when compared to other adsorbents, which demonstrates the potential of this sorbent for the purification process.

4. Conclusion

The results of this research demonstrate that the modified carbon dots, Zn-N-CDs, have a high capability to remove PO_4^{3-} from aqueous solutions. The key findings are summarized as follows: (i) The adsorption of PO_4^{3-} was strongly pH-dependent, with the highest adsorption capacity observed at pH 8. Increasing the ionic strength, up to around 100 mM KCl, significantly enhanced the adsorption capacity, with up to 78.82% of PO_4^{3-} removed. (ii) The adsorption process was found to be endothermic and spontaneous in nature. (iii) Zinc ions played a crucial role in buffering the solution and increasing PO_4^{3-} removal. The PO_4^{3-} was adsorbed in multilayers on the surface of Zn-N-CDs through ligand exchange and precipitation reactions.

Overall, the data presented in this study indicate that Zn-N-CDs could be a promising material for the removal of PO_4^{3-} from aquatic and terrestrial environments. However, the low yield and challenges in obtaining carbon dots as a solid powder due to their hydrophilic surface groups pose limitations on their large-scale use. Further research is needed to fully explore the potential of carbon dots in this field. Future studies should focus on assessing the impact of carbon dots on various biological species, such as microbes and aquatic organisms, in field-scale trials. Additionally, the effectiveness of phosphate removal by carbon dots in the presence of other impurities and potential compounds that may be present in real wastewater, such as organic matter and heavy metals, should be investigated.

Data availability

No primary research results, software or code have been included and no new data were generated or analysed as part of this review.

Author contributions

Mina Alikhani and Ehsan Khoshkalam designed and performed experiments and did all the data analysis and wrote this manuscript. Jalal Sadeghi did some laboratory experiments. Laura Bulgariu and Hossein Eshghi verified the analytical methods. All authors contributed to revising the manuscript.

Conflicts of interest

The authors declare no conflict of interest.

Acknowledgements

The authors declare that no funds, grants, or other support were received during the preparation of this manuscript. We are grateful to all of those with whom we have had the pleasure to work during this research. Also, we thank the chemistry department of Payame Noor University of Mashhad for providing laboratory space.

References

1 A. Nakarmi, S. E. Bourdo, L. Ruhl, S. Kanel, M. Nadagouda, P. Kumar, I. Pavel and T. Viswanathan, *J. Environ. Manage.*, 2020, **272**, 111048.
2 E. Zong, Y. Shen, J. Yang, X. Liu and P. Song, *ACS Omega*, 2023, **8**, 14177–14189.
3 D. A. Almasri, N. B. Saleh, M. A. Atieh, G. McKay and S. Ahzi, *Sci. Rep.*, 2019, **9**, 1–13.
4 M. R. Awual, *J. Clean. Prod.*, 2019, **228**, 1311–1319.
5 E. Khoshkalam, A. Fotovat, A. Halajnia, H. Kazemian and H. Eshghi, *J. Mol. Liq.*, 2023, **375**, 121366.
6 Y. Dai, Q. Sun, W. Wang, L. Lu, M. Liu, J. Li, S. Yang, Y. Sun, K. Zhang, J. Xu, W. Zheng, Z. Hu, Y. Yang, Y. Gao, Y. Chen, X. Zhang, F. Gao and Y. Zhang, *Chemosphere*, 2018, **211**, 235–253.
7 S. Wiriyathamcharoen, S. Sarkar, P. Jiemvarangkul, T. T. Nguyen, W. Klysuban and S. Padungthon, *Chem. Eng. J.*, 2020, **381**, 122671.
8 Q. Xu, W. Li, L. Ma, D. Cao, G. Owens and Z. Chen, *Sci. Total Environ.*, 2019, **703**, 135003.
9 H. Kong, Q. Li, X. Zheng, P. Chen, G. Zhang and Z. Huang, *Int. J. Biol. Macromol.*, 2023, **224**, 984–997.
10 P. Koilraj and S. Kannan, *J. Colloid Interface Sci.*, 2010, **341**, 289–297.
11 D. Guaya, H. Cobos, C. Valderrama and J. L. Cortina, *Nanomaterials*, 2022, **12**(20), 12203680.
12 G. Gallareta-Olivares, A. Rivas-Sanchez, A. Cruz-Cruz, S. M. Hussain, R. B. González-González, M. F. Cárdenas-Alcaide, H. M. N. Iqbal and R. Parra-Saldívar, *Chemosphere*, 2023, **312**(2022), 137190.
13 C. Long, Z. Jiang, J. Shangguan, T. Qing, P. Zhang and B. Feng, *Chem. Eng. J.*, 2021, **406**, 126848.
14 S. Sikiru, O. J. A. Abiodun, Y. K. Sanusi, Y. A. Sikiru, H. Soleimani, N. Yekeen and A. B. A. Haslija, *J. Environ. Chem. Eng.*, 2022, **10**, 108065.
15 R. Bhateria and R. Singh, *J. Water Process Eng.*, 2019, **31**, 100845.
16 S. J. Park, J. Y. Park, J. W. Chung, H. K. Yang, B. K. Moon and S. S. Yi, *Chem. Eng. J.*, 2020, **383**, 123200.

17 P. Devi, P. Rajput, A. Thakur, K. H. Kim and P. Kumar, *TrAC – Trends in Anal. Chem.*, 2019, **114**, 171–195.
18 A. Mehta, A. Mishra, S. Basu, N. P. Shetti, K. R. Reddy, T. A. Saleh and T. M. Aminabhavi, *J. Environ. Manage.*, 2019, **250**, 109486.
19 S. Y. Lim, W. Shen and Z. Gao, *Chem. Soc. Rev.*, 2015, **44**, 362–381.
20 M. Sabet and K. Mahdavi, *Appl. Surf. Sci.*, 2019, **463**, 283–291.
21 L. Wang, C. Cheng, S. Tapas, J. Lei, M. Matsuoka, J. Zhang and F. Zhang, *J. Mater. Chem. A*, 2015, **3**, 13357–13364.
22 M. Y. Pudza, Z. Z. Abidin, S. A. Rashid, F. M. Yasin, A. S. M. Noor and M. A. Issa, *Nanomaterials*, 2020, **10**(2), 10020315.
23 M. Alikhani, A. Mirbolook, J. Sadeghi and A. Lakzian, *Plant Physiol. Biochem.*, 2023, **200**, 107783.
24 J. Cheng, C. F. Wang, Y. Zhang, S. Yang and S. Chen, *RSC Adv.*, 2016, **6**, 37189–37194.
25 Y. Chen, H. Lian, Y. Wei, X. He, Y. Chen, B. Wang, Q. Zeng and J. Lin, *Nanoscale*, 2018, **10**, 6734–6743.
26 D. W. Li, X. F. Zhang, X. T. Zhang, X. Sen lv and N. You, *Opt Mater.*, 2023, **137**, 1–7.
27 R. Atchudan, T. N. J. I. Edison, S. Mani, S. Perumal, R. Vinodh, S. Thirunavukkarasu and Y. R. Lee, *Dalton Trans.*, 2020, **49**, 17725–17736.
28 S. K. Tammina, Y. Wan, Y. Li and Y. Yang, *J. Photochem. Photobiol., B*, 2020, **202**, 111734.
29 B. O. Isiuku, C. E. Enyoh, C. E. Duru and F. C. Ibe, *Curr. Res. Green Sustainable Chem.*, 2021, **4**, 100136.
30 B. Biswas, T. Rahman, M. Sakhakarmy, H. Jahromi, M. Eisa, J. Baltrusaitis, J. Lamba, A. Torbert and S. Adhikari, *Heliyon*, 2023, **9**, e19830.
31 Z. E. T. Teymoorian, N. Hashemi and M. H. Mousazadeh, *SN Appl. Sci.*, 2021, **305**(3), DOI: **10.1007/s42452-021-04287-z**.
32 Q. Xu, Y. Liu, R. Su, L. Cai, B. Li, Y. Zhang, L. Zhang, Y. Wang, Y. Wang, N. Li, X. Gong, Z. Gu, Y. Chen, Y. Tan, C. Dong and T. S. Sreeprasad, *Nanoscale*, 2016, **8**, 17919–17927.
33 Q. He, J. Ren and Y. Liu, *Nanotechnology*, 2022, **33**(17), DOI: **10.1088/1361-6528/ac4b7a**.
34 K. Yao, X. Lv, G. Zheng, Z. Chen, Y. Jiang, X. Zhu, Z. Wang and Z. Cai, *Environ. Sci. Technol.*, 2018, **52**, 14445–14451.
35 J. D. Clogston and A. K. Patri, *Methods Mol. Biol.*, 2011, **697**, 63–70.
36 X. Chen, H. Mi, C. Ji, C. Lei, Z. Fan, C. Yu and L. Sun, *J. Mater. Sci.*, 2020, **55**, 5510–5521.
37 C. Duan, T. Ma, J. Wang and Y. Zhou, *J. Water Process Eng.*, 2020, **37**, 101339.
38 D. Cao, X. Jin, L. Gan, T. Wang and Z. Chen, *Chemosphere*, 2016, **159**, 23–31.
39 H. Zhou, Y. Tan, Y. Yang, Y. Zhang, X. Lei and D. Yuan, *Appl. Clay Sci.*, 2021, **200**, 105903.
40 J. Antelo, M. Avena, S. Fiol, R. López and F. Arce, *J. Colloid Interface Sci.*, 2005, **285**, 476–486.
41 H. Kaya, R. B. Karabacak, Y. Çelik, J. Peake, S. Watkins, R. Sayer and E. Suvacı, *Microchem. J.*, 2023, **191**, 108772.
42 M. Talebi, R. Rahnemaie, E. Goli and M. Hossein, *Chem. Geol.*, 2016, **437**, 19–29.
43 Z. Ajmal, A. Muhmood, M. Usman, S. Kizito, J. Lu, R. Dong and S. Wu, *J. Colloid Interface Sci.*, 2018, **528**, 145–155.
44 J. C. Mendez and T. Hiemstra, *ACS Earth Space Chem.*, 2020, **4**, 545–557.
45 C. Tiberg and J. P. Gustafsson, *J. Colloid Interface Sci.*, 2016, **471**, 103–111.
46 S. M. Alardhi, A. H. Abdalsalam, A. A. Ati, M. H. Abdulkareem, A. A. Ramadhan, M. M. Taki and Z. Y. Abbas, *Polym. Bull.*, 2023, **81**, 1131–1157.
47 S. Kalam, S. A. Abu-Khamsin, M. S. Kamal and S. Patil, *ACS Omega*, 2021, **6**, 32342–32348.
48 Y. K. Choi, H. M. Jang, E. Kan, A. R. Wallace and W. Sun, *Environ. Eng. Res.*, 2019, **24**, 434–442.